

# Resurgence of Lunar Volcanism: Role of Localized Radioactive Enrichment in a Numerical Model of Magmatism and Mantle Convection

Ken'yo Uh<sup>1</sup>, Masanori Kameyama<sup>2,3</sup>, Gaku Nishiyama<sup>4,5,6</sup>, Takehiro Miyagoshi<sup>3</sup>, and Masaki Ogawa<sup>1</sup>

<sup>1</sup>Department of Earth Sciences and Astronomy, The University of Tokyo, Komaba, Meguro, Japan

<sup>2</sup>Geodynamics Research Center, Ehime University, Matsuyama, Japan

<sup>3</sup>Japan Agency for Marine-Earth Science and Technology, Yokohama, Japan

<sup>4</sup>Institute of Planetary Research, German Aerospace Center, Berlin, Germany

<sup>5</sup>Department of Earth and Planetary Science, The University of Tokyo, Hongo, Bunkyo, Japan

<sup>6</sup>RISE project, National Astronomical Observatory of Japan, Osawa, Mitaka, Japan

## Key Points:

- To understand the localized long-lasting volcanism of the Moon, we developed a numerical model of magmatism in the convecting mantle
- The calculated volcanic activity has two peaks caused by ascent of partially molten plumes from the deep mantle to the uppermost level
- Localized radioactive enrichment in the uppermost mantle plays an important role in the long-lasting volcanism with a couple of peaks

arXiv:2407.07505v1 [physics.geo-ph] 10 Jul 2024

---

Corresponding author: Ken'yo Uh, [u-kenyo0822@g.ecc.u-tokyo.ac.jp](mailto:u-kenyo0822@g.ecc.u-tokyo.ac.jp)

**Abstract**

We develop a 2-D numerical model of magmatism and mantle convection to understand the volcanism on the Procellarum KREEP terrane (PKT) of the Moon, which continued for billions of years with two peaks of activities at 3.5-4 Gyr ago and around 2 Gyr ago. In our model, the effects of the PKT on lunar evolution are considered by initially imposing a region of localized radioactive enrichment. The calculated volcanism has two peaks induced by different mechanisms. The first peak occurs at 3.5-4 Gyr ago when magma generated in the deep mantle by internal heating ascends to the surface as partially molten plumes. The basaltic blocks in the uppermost mantle formed by this magmatism, then, sink to the deep mantle, triggering further plumes that cause the resurgence of volcanism at  $\sim 2$  Gyr ago. Our model shows that localized radioactive enrichment is important for the long-lasting volcanism with a couple of peaks.

**Plain Language Summary**

Geological observations of the Moon have revealed that volcanism continued for billions of years in the Procellarum KREEP Terrane (PKT), a region enriched in radioactive heat-producing elements (HPEs); this long-lasting localized volcanism had peaks at 3-4 Gyr and around 2 Gyr ago. However, it remains unclear how volcanism has been maintained for so long. Here, we calculated a 2-D model of magmatism and mantle convection, considering a localized radioactive enrichment (EA) beneath the crust to model the PKT. Our simulations show that the first and second peaks of localized volcanism were induced by the ascent of partially molten plumes, but driven by different mechanisms. The first peak of the volcanism is accounted for by ascending partially molten plumes that are generated by strong internal heating at the base of the mantle. The second peak of the volcanism is driven by the descent of basaltic blocks formed by the earlier magmatism; the compositionally dense basaltic blocks founder into the deep mantle, triggering further partially molten plumes beneath the EA from 1.2 to 2.8 Gyr. Our model shows that localized radioactive enrichment in the uppermost mantle plays a critical role in the long-lasting volcanism of the Moon.

**1 Introduction**

Understanding the volcanism of the Moon has been a long-standing issue in studies of lunar mantle evolution (e.g., Solomon & Chaiken, 1976; Kirk & Stevenson, 1989; Arai et al., 2008; Head et al., 2023). Geological observations have revealed that volcanism has been particularly active in the Procellarum KREEP Terrane (PKT) located on the nearside, which is enriched in radioactive heat-producing elements (HPEs) (e.g., Jolliff et al., 2000; Lawrence et al., 2000; Wieczorek & Phillips, 2000; Kamata et al., 2013). Volcanism has occurred in other regions but has been less active (e.g., Shearer et al., 2006). In the PKT, volcanic activity continued for several billion of years with a peak at 3.5-4 Gyr ago (e.g., Hiesinger et al., 2000, 2003; Hurwitz et al., 2013; Whitten & Head, 2015; Nagaoka et al., 2020; Che et al., 2021; Su et al., 2022). This period of active volcanism coincides with the time of the radial expansion of the Moon: the Moon expanded globally by 0.5–5 km until around 3.8 Gyr ago (e.g., Andrews-Hanna et al., 2013, 2014; Liang & Andrews-Hanna, 2022; Sawada et al., 2016) and then contracted globally over time (Yue et al., 2017; Frueh et al., 2023), by around 1 km or less in the past 1 Gyr (e.g., Waters et al., 2010, 2015; Klimczak, 2015; Clark et al., 2017). The volcanic activity in the PKT, however, did not decline monotonically after the peak; it revived at around 2 Gyr ago (e.g., Morota et al., 2011; Cho et al., 2012; Kato et al., 2017; Giguere et al., 2022). To understand the long-lasting history of lunar volcanism with two peaks in its activity, which mostly occurs in the PKT, we used a 2-D polar rectangular model of magmatism in the convecting lunar mantle (U et al., 2023).

Various numerical models have been developed to account for the long-lasting volcanism of the Moon (e.g., Solomon & Head, 1979; Wilson & Head, 2003; Breuer & Moore, 2015). Some numerical models, in which the surface is covered by the HPE-enriched crust or a regolith layer as a blanket layer, suggest that magma persists in the uppermost mantle for 1-2 Gyr (e.g., Konrad & Spohn, 1997; Spohn et al., 2001; Ziethe et al., 2009). This partially molten region, however, extends globally and is unlikely to have caused the localized volcanism at the PKT. Some earlier researchers suggest that the localized volcanism is caused by one or some hot plumes growing from a layer of ilmenite-bearing cumulates (IBC) enriched in HPEs that developed on the core-mantle boundary (CMB) in the lunar early history (e.g., Stegman et al., 2003; de Vries et al., 2010; N. Zhang et al., 2013a, 2017; W. Zhang et al., 2022, 2023) owing to the magma ocean and mantle overturn (e.g., Hess & Parmentier, 1995; Ringwood & Kesson, 1976). Although the plume enriched in the IBC component ascends by thermal buoyancy in these models, it is unclear if the large excess density of the IBC component, as expected from earlier models of mantle overturn, allows the ascent of such a compositionally dense plume in the Moon (e.g., Le Bars & Davaille, 2004; H. Li et al., 2019; Yu et al., 2019; Zhao et al., 2019). On the other hand, Wieczorek and Phillips (2000) and Laneuville et al. (2013, 2018) assumed a locally HPE-enriched area at the top of the mantle in the initial condition and found that the area remained partially molten for more than 3 Gyr. In these models, however, the extraction of HPEs from the partially molten area by segregating magma (Cassen & Reynolds, 1973; Cassen et al., 1979) is neglected, and HPEs remain in the uppermost mantle throughout the calculated 3 Gyr. Ogawa (2018a) found that partially molten regions solidify within 2 Gyr when HPE-extraction by magmatism is considered.

To understand the mantle evolution of the Moon, constrained by its volcanic history as well as radial expansion/contraction history, we extend the 2-D model of magmatism and mantle convection that we have developed (U et al., 2023). In this model, magma is generated by decompression melting and internal heating, then migrates upward in partially molten regions as a permeable flow through the coexisting matrix; thermal, compositional, and melt buoyancy drive mantle convection in a Newtonian fluid with temperature-dependent viscosity; heat, mass, and incompatible HPEs are transported by magma. In our earlier study, we initiated the calculation with a compositionally stratified mantle, enriched with the IBC component at the base of the mantle (U et al., 2023) following earlier studies of the magma ocean: during the last stage of crystallization of the lunar magma ocean, a dense IBC layer enriched in KREEP (K, rare earth elements, and P-rich material) develops at the top of the mantle and subsequently sinks to the CMB, a process called mantle overturn (e.g., Alley & Parmentier, 1998; Hess & Parmentier, 1995; Boukaré et al., 2018). In addition to this initial stratification, we also consider a localized enrichment of HPEs beneath the crust to model the PKT and investigate whether this enriched area (EA) induces a localized volcanism similar to that observed at the PKT (Figure 1a).

## 2 Model descriptions

We used the 2-D annular model of mantle convection and magmatism developed in U et al. (2023). The finite difference numerical code calculates the energy, mass, and momentum equations of mantle convection in  $R = [(r, \theta) | 385 \text{ km} \leq r \leq 1735 \text{ km}, 0 \leq \theta \leq \pi]$  on a mesh with 128 (radial direction) times 256 (lateral direction) mesh points, under the Boussinesq approximation. (See Section S1 of Supporting Information for the detail of the basic equations.) To model the blanket effect of the crust (Ziethe et al., 2009), we reduced the thermal diffusivity by a factor of two in a blanket layer 35 km thick at the top of the mantle. The core is modeled as a heat bath with a uniform temperature, and its heat capacity is 0.01 times that of the mantle (Kameyama et al., 1996). The vertical sidewalls are insulated, while the surface boundary is fixed at 270 K; all boundaries are shear stress-free and impermeable to both magma and matrix.

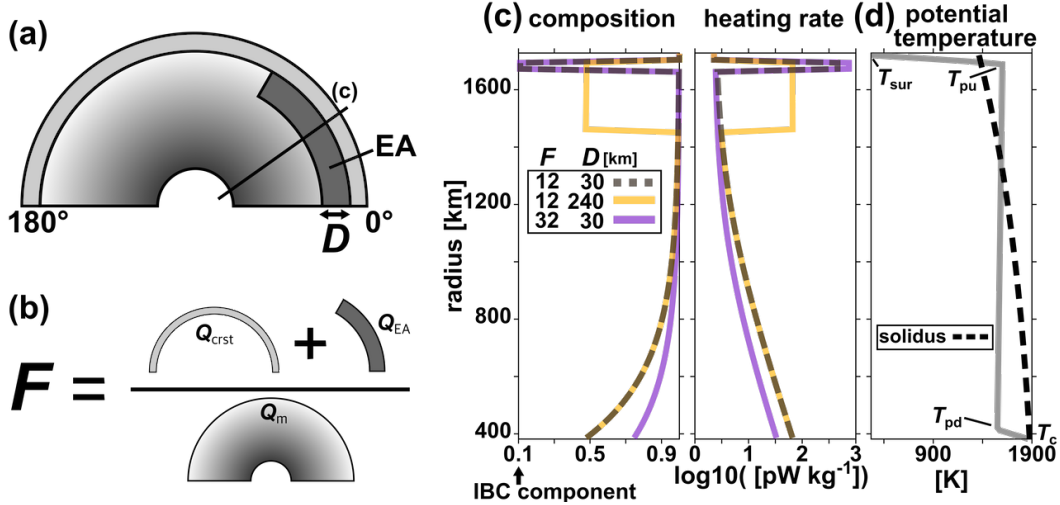


**Figure 1.** (a, b) An illustration of the initial distribution of heat-producing elements (HPEs). The distribution is laterally uniform except for the enriched area ‘EA’. In (b)  $F$  is the ratio of the total amount of HPEs in the crust  $Q_{\text{crst}}$  and the EA  $Q_{\text{EA}}$  to that in the mantle  $Q_{\text{m}}$  (see Section S1-2 in Supporting Information). Also shown are (c) the initial distribution of the composition and heating rate along the line in (a); (d) the initial distribution of the potential temperature ( $T_{\text{sur}} = 270$  K,  $T_{\text{pu}} = 1600$  K,  $T_{\text{pd}} = 1550$  K, and  $T_{\text{c}} = 1875$  K are assumed in this figure).

The convecting material is a binary eutectic system composed of an olivine-rich material with a density of  $3300 \text{ kg m}^{-3}$  and an IBC material with a density of  $3745 \text{ kg m}^{-3}$  (e.g., Snyder et al., 1992; Elkins-Tanton et al., 2011; Liang et al., 2024). The content of the olivine-rich component is denoted by  $\xi$ ; the eutectic composition is at  $\xi_{\text{e}} = 0.1$ , corresponding to the basaltic composition. The bulk composition  $\xi$  is calculated from the composition of the solid phase  $\xi_{\text{s}}$  and that of the liquid phase  $\xi_{\text{l}}$  written as

$$\xi = (1 - \phi) \xi_{\text{s}} + \phi \xi_{\text{l}}, \quad (1)$$

where  $\phi$  is the melt-content. The solidus and liquidus temperatures are calculated from the phase diagram assumed for the binary eutectic system (see Appendix A in U et al. (2023)). The convecting material contains HPEs that decay with time. Magmatism is modeled by the generation and upward migration of magma as a permeable flow (e.g., McKenzie, 1984; Katz, 2008; Miller et al., 2014). The flow is driven by the buoyancy of magma, and the relative velocity between the velocity of melt  $\mathbf{u}$  and that of matrix  $\mathbf{U}$  is calculated from

$$\mathbf{u}^* - \mathbf{U}^* = -Mg^* \frac{\phi^2}{\phi_0^3} (\rho_{\text{s}}^* - \rho_{\text{l}}^*) \mathbf{e}_{\text{r}}, \quad (2)$$

where the asterisks stand for normalized quantities.  $\rho_{\text{s}} - \rho_{\text{l}}$  is the density difference between solid and melt phases calculated as

$$\rho_{\text{s}}^* - \rho_{\text{l}}^* = \beta (\xi_{\text{l}} - \xi_{\text{s}}) + \frac{\Delta v_1}{v_0} [1 + \beta (1 - \xi_1)] \quad (3)$$

(See Eqs. S6, S7 in Supporting information). Here,  $g$  is the gravitational acceleration;  $\phi_0 = 0.05$  is the reference melt-content;  $\Delta v_1/v_0$  is the amount of density reduction by melting described in Eq. 5 of U et al. (2023). We assumed the reference permeability  $M^*$  as

$$M^* \equiv \frac{k_{\phi_0} \rho_0 g_0 L}{\kappa \eta_{\text{melt}}} \simeq 100, \quad (4)$$

where the parameter values are listed in Table S1.  $\beta = 0.135$  is a constant that expresses the sensitivity of density to the bulk composition. In most cases, we assumed that the crustal density is higher than the density of magma for simplicity. However, the density of the lunar crust is lower than that of basaltic magma (e.g., Morota et al., 2009; Taguchi et al., 2017; Wilson & Head, 2017; Head & Wilson, 2017, 2020), and Lourenço et al. (2018) suggest that the thermal history of the Moon can substantially depend on the crustal density inversion. To clarify the effect of the density inversion, we increased the value of  $\beta$  to 0.253 in the blanket layer in a case (Case crst-F12-D30): the crustal density is  $2550 \text{ kg m}^{-3}$  (Wieczorek et al., 2013) which is lower than the density of the basaltic magma at this value of  $\beta$ .

To simulate the localized enrichment of HPEs in the mantle beneath the PKT, we assumed an enriched area (EA) in  $[(r, \theta) \mid 1700 - D \text{ km} \leq r \leq 1700 \text{ km}, 0 \leq \theta \leq 1/3 \pi]$  that is enriched in HPEs and the IBC component, as illustrated in Figure 1a. We examined the dependence of calculated volcanism on the thickness of the EA ‘ $D$ ’ and on the ratio of the total amount of HPEs in the crust and the EA to the mantle ‘ $F$ ’ (Figure 1a, b); note that HPE-content in the crust is constant for simplicity (see Section S1-2 in Supporting Information). The searched range of ‘ $D$ ’ (10-240 km) is estimated from the thickness of the KREEP layer that remains after the mantle overturn (Laneuville et al., 2013, 2018; Charlier et al., 2018; Schwinger & Breuer, 2022; N. Zhang et al., 2022; Jones et al., 2022). We also take the searched range of ‘ $F$ ’ (4-32) from the estimates in Spohn et al. (2001).

In the initial condition, we assumed that the mantle is compositionally stratified to simulate the layering of the lunar mantle inferred from previous studies of the magma ocean and mantle overturn (e.g., Parmentier et al., 2002; Hess & Parmentier, 1995). The contents of HPEs and the IBC component increase exponentially with depth as illustrated in Figure 1c. The average of the internal heating rate over the entire mantle is  $q_0 = 14.7 \text{ pW kg}^{-1}$  at 4.4 Gyr estimated from Table S2 in Section S1-1. The initial temperature distribution (Figure 1d) is also taken from earlier models of the lunar mantle overturn (e.g., Boukaré et al., 2018; Yu et al., 2019; Zhao et al., 2019) and the evolution model (U et al., 2022). The details of the initial condition are described in Section S1-2.

### 3 Results

In Figures 2 and 3 as well as the animation (Movie S1 in the supporting file), we present the evolution of the mantle calculated in Case F12-D30 where  $F = 12$  and  $D = 30 \text{ km}$  (see also figures in Supporting Information).

Magma is generated in the deep mantle owing to the strong internal heating assumed in the initial condition (Figure 1c) and migrates upward as partially molten plumes to reach the uppermost mantle within the first 0.7 Gyr (Figures 2b, c; see also Figure S1a); melt buoyancy is the main driving force of this flow. Magma rises to the depth level of 100 km beneath the EA in  $[0 \leq \theta \leq 1/3 \pi]$ , which is shallower than beneath the area outside the EA (Figures 3a, b). This is because the lithosphere is thinned beneath the EA owing to the strong heating by HPEs in the EA (Figure 2a, c). The magma transports HPEs and the basaltic component to the uppermost mantle, forming basaltic blocks (see the arrows in Figure 2d for 0.76 Gyr). A deeper part of the compositionally dense basaltic blocks eventually founders to the CMB as magma accumulates and the blocks grow (see the arrow in Figure 2d for 1.12 Gyr). We found that the core temperature drops by about 40 K in 100 Myr as the cold basaltic blocks descend to the CMB (see Figure S1b, c). The descending basaltic blocks trigger further ascent of partially molten plumes from the deep mantle driven by melt buoyancy, as depicted by the arrows in Figures 2b. Accordingly, the upward magma flux beneath the EA becomes significant again from 1.2 to 2.8 Gyr (Figure 3b). The resurgence of magma flux is not found in our earlier models that are devoid of the EA (see the gray dotted line in Figure 3b). In contrast, the

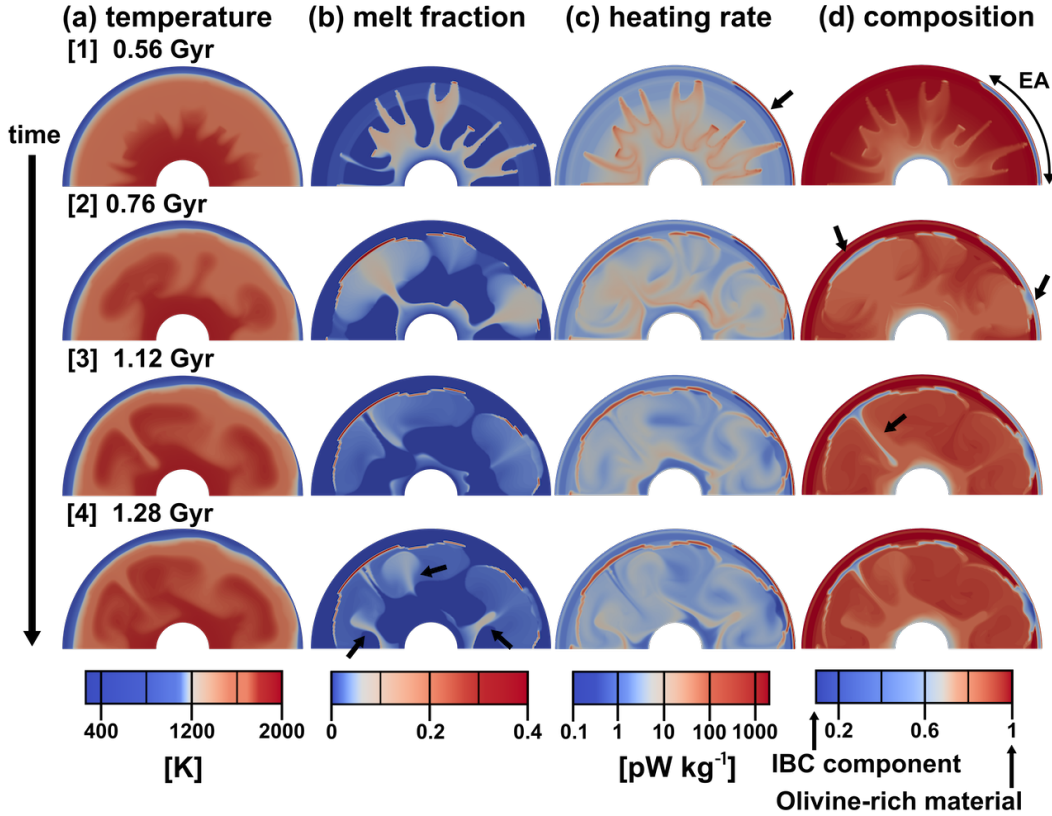


**Figure 2.** Snapshots of the distributions of (a) temperature, (b) melt-content, (c) internal heating rate, and (d) bulk composition calculated for the reference case ( $F = 12$  and  $D = 30$  km; Case F12-D30). The elapsed times are indicated in the figure. In (d), the blue color stands for the basaltic composition enriched in the IBC component, while the red color stands for the olivine-rich end-member. The numbers [1] to [4] correspond to those of Figure 3b.

magma flux is negligibly small throughout the calculated history outside the EA due to the thicker lithosphere (Figure 3a, b). After 2.8 Gyr, the partially molten region in the mantle shrinks with time due to the decay of HPEs but persists until 4.4 Gyr (Movie S1 as well as Figure S1d). From further numerical experiments with various values of  $D$  in the range of 10-240 km and  $F$  in the range of 4-32, we found that the localized volcanism revives and continues for more than 1.5 Gyr in the cases with  $D < 120$  km and  $8 < F < 24$  (see Section S2-2 including Table S3 and Figure S2 in Supporting Information).

The resurgence of magma flux beneath the EA observed in the reference case is more pronounced in Case crst-F12-D30 where the crustal density is lower than the density of the basaltic magma (see Figure 3c, d as well as Figure S3). The upward magma flux shown in Figure 3c is substantial beneath the entire EA until 3.7 Gyr, and magma enriched in HPEs remains along the crust-mantle boundary even at as late as 3.5 Gyr (Figure S3). The resurgence of magma flux is so significant in crst-F12-D30 because the lower density of the crust prevents magma from transporting HPEs to the surface; HPEs remain beneath the crust to keep the lithosphere beneath the EA thinner compared with that in the reference case.



We found that strong internal heating and compositionally high density in the EA, as well as initial mantle stratification, are important for the resurgence of magma flux beneath the EA (see Figure S4-S7). The resurgence of magma flux is not observed in Case noHeat-F12-D30 where the enrichment of HPEs in the EA is not considered (Figures S4a and S5). The resurgence occurs only briefly in Case noBa-F12-D30 where the compositional high density in the EA is not considered (Figures S4b and S6). This is due to the smaller density difference between the mantle and magma  $\rho_s - \rho_l$  in the EA compared to the reference case, resulting in lower permeable flow there (Eqs. 2 and 3). On the other hand, magma flux at the depth level of 100 km is not observed since 0.5 Gyr after the start of the calculation in Case noStra-F12-D30 where the HPEs and the composition  $\xi$  are vertically uniform in the initial mantle (Figures S4c and S7). The deep mantle is not enriched in HPEs in this case, and sufficient magma generation does not occur to ascend to the uppermost mantle.

Figure 3e shows that the Moon expands globally by more than 3 km for the first 0.7 Gyr of the calculated history and then contracts at a rate of around  $-1 \text{ km Gyr}^{-1}$  in the past 1 Gyr in the reference case. The decomposition of radius change  $\Delta R$  into the component caused by melting/solidification and by thermal expansion/contraction shows that the expansion is mainly caused by melting, while the contraction is mainly caused by thermal contraction (Figure S8). The overall feature of the radius change is not affected by the crustal density (see the black dotted line in Figure 3e). However, there is a drop in the radius beneath the EA  $\Delta R_{EA}$  at around 3.7 Gyr due to the solidification of the mantle in Case crst-F12-D30 (see Figure S9). This is because a partially molten region that persists until that time along the crust-mantle boundary beneath the EA solidifies (Figure 3c; see also Figure S3).

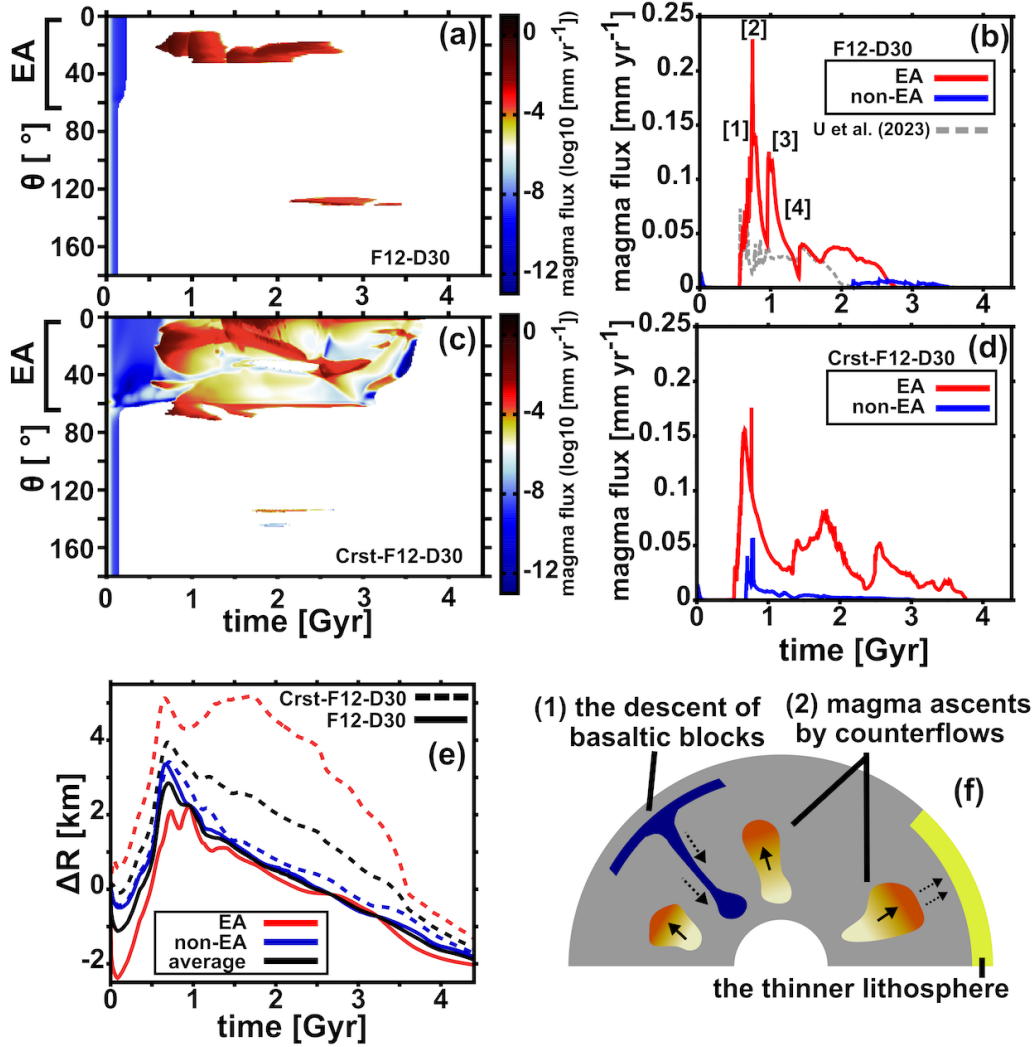
## 4 Discussions

Figure 3f illustrates how an enriched area (EA) causes a long-lasting volcanism in our models. In the earlier stage of mantle evolution, magma is generated in the deep mantle by internal heating and ascends to the uppermost mantle as partially molten plumes. In the area beneath the EA, magma rises to a shallower depth than in the area outside the EA because the lithosphere there is thinner owing to the strong internal heating assumed in the initial condition. This magmatism results in the formation of basaltic blocks beneath the lithosphere. The basaltic blocks outside the EA eventually sink to the CMB, triggering further plume activity that causes to a second peak in volcanism.

### 4.1 Comparison With Earlier Models of Lunar Volcanic History

A comparison with earlier mantle convection models of lunar volcanic history, which mostly occurs in the PKT and its surrounding area, shows the crucial role of melt buoyancy in our models. Some models suggest that localized volcanism is caused by thermal plumes from an HPE-enriched IBC layer on the CMB (e.g., Zhong et al., 2000; N. Zhang et al., 2013b). In these models, however, the compositional density contrast between the basal IBC layer and the overlying olivine-rich mantle is substantially less than  $160 \text{ kg m}^{-3}$  (see Figure 6 in H. Li et al. (2019)), the value suggested from some recent mantle overturn models (e.g., Yu et al., 2019; Zhao et al., 2019; Maurice et al., 2024). At this density contrast, the basal layer remains convectively stable and does not rise as a plume by thermal buoyancy alone (Le Bars & Davaille, 2004; de Vries et al., 2010). In contrast, a large fraction of the IBC component in the deep mantle arises as partially molten plumes mostly driven by melt buoyancy in our models (Figure 2) although the density contrast is more than  $200 \text{ kg m}^{-3}$  in our reference case (Figure 1c).

Our models also suggest the reason why volcanism continues so long in the PKT. In some of earlier models, a locally HPE-enriched area at the top of the mantle assumed in the initial condition remains partially molten for more than 3 Gyr (Wieczorek & Phillips,



**Figure 3.** (a) The distribution of the upward flux of magma that passes upward through the depth level of 100 km and (b) the average flux of magma around the EA (the red line) and outside the EA (the blue line) at the depth level of 100 km in Case F12-D30 (the reference case). Also shown are (c & d) the magma flux calculated in Case crst-F12-D30 where the crust is less dense than basaltic magma; (e) the history of radius change  $\Delta R$  calculated by Eq. S17 in Section S1-3; (f) a schematic illustration of long-lasting volcanism with a couple of peaks in the PKT calculated in the model. In (b, d, and e), the blue lines and red lines stand for the average values in  $[0 \leq \theta \leq 1/3\pi]$  (beneath the EA) and in  $[1/3\pi < \theta \leq \pi]$  (outside the EA), respectively, while the black lines stand for the total average values in  $[0 \leq \theta \leq \pi]$ . In (b), the gray line shows the magma flux in our earlier model (U et al., 2023) where the EA is not considered (other parameters are the same as those assumed in Case F12-D30); the numbers [1]–[4] correspond to those of Figure 2.



2000; Laneuville et al., 2013, 2018). HPE-extraction from the enriched area by magmatism is, however, neglected in these models as we discussed before. In our models, magmatism continues long despite that HPE-transport by magma is taken into account, because the basaltic blocks formed by early magmatism descend to the CMB to trigger further ascent of partially molten plumes (Figures 2 and 3a, f). Besides, the melting history of the uppermost mantle depends on the crustal density. In Case crst-F12-D30 where the crustal density is lower than the density of the basaltic magma, HPEs are not extracted to the surface but remain at the base of the crust (see Figure S3). The HPEs at the crust-mantle boundary keep the lithosphere thin enough for revived plume activity to cause volcanism. The resurgence of magma flux is so significant beneath the entire EA for more than 3.5 Gyr due to the plume activity (Figure 3c, d). By comparing magma flux under varying initial conditions (Figures S4-S7), our simulations also show that both the initial mantle stratification and the EA beneath the crust play crucial roles in the resurgence of volcanism after 1 Gyr. Note that a detailed discussion of volcanic history is possible in our models because we calculate the magma flux directly, rather than estimating it from the distribution of magma in the mantle, as is done in earlier models (e.g., Wood, 1972; Solomon & Toksöz, 1973; Konrad & Spohn, 1997; U et al., 2022).

## 4.2 Comparison With the Observed Features of the Moon

The magma flux beneath the EA shown in our reference case is consistent with the observed history of volcanism in the PKT. Magma generated at depth by strong internal heating rises (Figure 2 for 0.56 Gyr and 0.76 Gyr), causing the peak of volcanism at 3.5-4 Gyr ago (e.g., Hiesinger et al., 2000; Whitten & Head, 2015). The resurgence of volcanism triggered by the descending basaltic blocks is consistent with the observed volcanic history in the PKT with the second peak at around 2 Gyr ago (e.g., Cho et al., 2012; Tian et al., 2023). The early expansion and later contraction of the planet in the reference case (Figure 3e) are also consistent with those suggested from gravity gradiometry data and tectonic features (e.g., Andrews-Hanna et al., 2013; van der Bogert et al., 2018; Matsuyama et al., 2021). The plumes triggered by descending basaltic blocks are depleted in HPEs compared to the plumes that ascend in the early history (see the frames of 0.76 Gyr and 1.28 Gyr in Figure 2c, d; see also the animation). The plume activity in the later history can account for the HPE-depleted young basalts observed in the PKT (Che et al., 2021; Q.-L. Li et al., 2021; Su et al., 2022). It is, however, difficult to account for the temporal trend of increasing Ti content in the HPE-depleted mare basalts in the PKT after around 2.3 Gyr ago (Kato et al., 2017; Sato et al., 2017; D. Zhang et al., 2022). This trend may be due to the remelting of basaltic blocks in the uppermost mantle by the plumes that rise later (Figures 2). To clearly understand this trend, it is necessary to carefully model magma evolution caused by fractional crystallization (e.g., Luo et al., 2023).

In all of our calculated models, the heat flux on the CMB  $q_{\text{CMB}}$  is too low to drive the long-lasting core dynamo in all of our calculated models. In the reference model, the heat flux is close to 0  $\text{mW m}^{-2}$  since the first few hundred million years (see Figure S1c). The same conclusion has been reached in many of previous mantle convection models (e.g., Konrad & Spohn, 1997; Laneuville et al., 2013; Maurice et al., 2024). A previous model proposes that  $q_{\text{CMB}}$  becomes temporally high enough to induce the core dynamo when the IBC-rich layer on the CMB is internally heated and rises as plumes by thermal buoyancy (Stegman et al., 2003). Although hot plumes rise from the IBC-rich layer in our model too, a part of the layer remains on the CMB for more than 800 Myr to keep  $q_{\text{CMB}}$  around 0  $\text{mW m}^{-2}$  (Figure 2a, b for 0.76 Gyr; see also Figure S1b).  $q_{\text{CMB}}$  temporally increases only slightly at around 1.4 Gyr as cold basaltic blocks sink to the CMB (see Figure S1c). The flux is too small to drive the core dynamo (e.g., Christensen et al., 2009; Weiss & Tikoo, 2014). It is likely that dynamo mechanisms other than secular cooling of the core are needed to sustain the long-lasting core dynamo throughout the history of the Moon, such as core crystallization (e.g., Laneuville et al., 2014; Evans et al.,

2018), a basal magma ocean (Scheinberg et al., 2018; Hamid et al., 2023), and precession of the rotation axis (e.g., Dwyer et al., 2011; Stys & Dumberry, 2020). It is also important to re-examine the history of magnetic fields on the Moon (e.g., Tikoo et al., 2017; Tarduno et al., 2021; Jung et al., 2024).

Further calculations in a 3-D spherical mantle are important to more quantitatively predict the history of magma flux, radial expansion/contraction, and thermal history of the Moon and to compare the predictions with such observations as the temperature distribution in the Moon (e.g., Khan et al., 2006, 2014). As already found by Guerrero et al. (2018) for the Moon, 2-D polar rectangular models of mantle convection tend to predict higher average mantle temperatures compared to 3-D spherical models, especially when the core size is small. In the reference case, the mid-mantle temperature at 4.4 Gyr is about 100 K higher than current lunar estimates (Figure S1d), which may result from the geometry of the convecting vessel.

## 5 Conclusions

To understand the long-lasting localized volcanism in the PKT (the Procellarum KREEP terrane) with the first peak at 3-4 Gyr ago and the second one at about 2 Gyr ago, we numerically simulated a 2-D polar rectangular model of magmatism and mantle convection where a localized heat-producing elements (HPEs) enrichment beneath the crust, called enriched area (EA) is considered to model the PKT in the initial mantle stratification (Figure 1).

Our simulations show that the first and second peaks of localized volcanism, occurring at about 1 Gyr intervals, were induced by ascent of partially molten plumes driven by different mechanisms. The first peak of the volcanism is accounted for by magma ascent as partially molten plumes from the deep mantle induced by internal heating there (Figures 2 and 3b). Magma ascends to the uppermost mantle beneath the EA because the lithosphere there is thinned by the strong internal heating in the EA. The second peak of the volcanism, in contrast, is caused by counterflows driven by the descent of basaltic blocks formed by the earlier magmatism beneath the lithospheric lid; a deeper part of the compositionally dense basaltic blocks sinks into the deep mantle owing to their negative buoyancy, triggering further magma ascent beneath the EA from 1.2 to 2.8 Gyr (Figure 3b, f). We found that the mantle evolves as illustrated in Figure 3f when the thickness of the EA is  $D < 120$  km and the ratio of the total amount of HPEs in the crust and the EA to the mantle is  $8 < F < 24$  (see Table S3). Our models suggest that material transport and melt buoyancy by magmatism play critical roles in the lunar mantle evolution. To reproduce the long-lasting volcanism with a couple of peaks in the PKT, localized radioactive enrichment in the uppermost mantle is important.

## Data Availability Statement

The official version of the animations and Supporting Information as well as dataset will be made available if it has been accepted by GRL. However, the unofficial version of the animation and Figures S1-S9 can be accessed via the following links.

<https://youtu.be/Mdhh9a7P-zY>

<https://youtu.be/m1dCnxtrIge>

## References

- Alley, K. M., & Parmentier, E. M. (1998). Numerical experiments on thermal convection in a chemically stratified viscous fluid heated from below: implications for a model of lunar evolution. *Phys. Earth Planet. Inter.*, *108*(1), 15–32. doi:

10.1016/S0031-9201(98)00096-X

- Andrews-Hanna, J. C., Asmar, S. W., Head III, J. W., Kiefer, W. S., Konopliv, A. S., Lemoine, F. G., ... Zuber, M. T. (2013). Ancient igneous intrusions and early expansion of the moon revealed by grail gravity gradiometry. *Science*, *339*, 675–678. doi: 10.1126/science.1231753
- Andrews-Hanna, J. C., Besserer, J., Head III, J. W., Howett, C. J. A., Kiefer, W. S., Lucey, P. J., ... Zuber, M. T. (2014). Structure and evolution of the lunar procellarum region as revealed by grail gravity data. *Nature*, *514*, 68–71. doi: 10.1038/nature13697
- Arai, T., Terada, H., Yamaguchi, A., & Ohtake, M. (2008). A new model of lunar crust: asymmetry in crustal composition and evolution. *Earth Planets Space*, *60*, 433–444. doi: 10.1186/BF03352808
- Boukaré, C.-E., Parmentier, E. M., & Parman, S. W. (2018). Timing of mantle overturn during magma ocean solidification. *Earth Planet. Sci. Lett.*, *491*(1), 216–225. doi: 10.1016/j.epsl.2018.03.037
- Breuer, D., & Moore, W. (2015). 10.08 - dynamics and thermal history of the terrestrial planets, the moon, and io. *Treatise on Geophysics (Second Edition)*, In G. Schubert (Ed.), 255–305. doi: doi.org/10.1016/B978-0-444-53802-4.00173-1
- Cassen, R., & Reynolds, R. T. (1973). Role of convection in the moon. *J. Geophys. Res.*, *78*(17), 3203–3215. doi: 10.1029/JB078i017p03203
- Cassen, R., Reynolds, R. T., Graziani, F., Summers, A., McNellis, J., & Blalock, L. (1979). Convection and lunar thermal history. *Phys. Earth Planet. Inter.*, *19*(2), 183–196. doi: 10.1016/0031-9201(79)90082-7
- Charlier, B., Grove, T. L., Namur, O., & Holtz, F. (2018). Crystallization of the lunar magma ocean and the primordial mantle-crust differentiation of the moon. *Geochim. Cosmochim. Acta*, *234*, 50–69. doi: 10.1016/j.gca.2018.05.006
- Che, X., Nemchin, A., Liu, T., D. Long, Norman, M. D., Joy, K. H., Tartese, R., ... more (2021). Age and composition of young basalts on the moon, measured from samples returned by chang’e-5. *Science*, *374*(6569), 887–890. doi: 10.1126/science.abl7957
- Cho, Y., Morota, T., Haruyama, J., Yasui, M., Hirata, N., & Sugita, S. (2012). Young mare volcanism in the orientale region contemporary with the procellarum krep terrane (pkt) volcanism peak period around 2 billion years ago. *Geophys. Res. Lett.*, *39*(11). doi: 10.1029/2012GL051838
- Christensen, U. R., Holzwarth, V., & Reiners, A. (2009). Energy flux determines magnetic field strength of planets and stars. *Nature*, *457*(7226), 167–169. doi: 10.1038/nature07626
- Clark, J. M., Jaclyn D. Hurtado Jr., Hiesinger, H., van der Bogert, C. H., & Bernhardt, H. (2017). Investigation of newly discovered lobate scarps: Implications for the tectonic and thermal evolution of the moon. *Icarus*, *298*, 78–88. doi: 10.1016/j.icarus.2017.08.017
- de Vries, J., van den Berg, A., & van Westrenen, W. (2010). Formation and evolution of a lunar core from ilmenite-rich magma ocean cumulates. *Earth Planet. Sci. Lett.*, *292*(1-2), 139–147. doi: 10.1016/j.epsl.2010.01.029
- Dwyer, C., Stevenson, D., & Nimmo, F. (2011). A long-lived lunar dynamo driven by continuous mechanical stirring. *Nature*, *479*(7372), 212–214. doi: 10.1038/nature10564
- Dyger, N., Hirth, G., & Liang, Y. (2016). A flow law for ilmenite in dislocation creep: Implications for lunar cumulate mantle overturn. *Geophys. Res. Lett.*, *43*(2), 532–540. doi: 10.1002/2015GL066546
- Elkins-Tanton, L., Burgess, S., & Yin, Q.-Z. (2011). The lunar magma ocean: reconciling the solidification process with lunar petrology and geochronology. *Earth Planet. Sci. Lett.*, *304*(3–4), 326–336. doi: 10.1016/j.epsl.2011.02.004
- Evans, A. J., Tikoo, S. M. ., & Andrews-Hanna, J. C. (2018). The case against an early lunar dynamo powered by core convection. *Geophys. Res. Lett.*, *45*(1),

- 98–107. doi: 10.1002/2017GL075441
- Frueh, T., Hiesinger, H., Bogert, C. H., Clark, J. D., Watters, T. R., & Schmedemann, N. (2023). Timing and origin of compressional tectonism in mare tranquillitatis. *J. Geophys. Res. Planets*, *128*(e2022JE007533). doi: 10.1029/2022JE0075
- Garcia, R. F., Gagnepain-Beyneix, J., Chevrot, S., & Lognonné, P. (2011). Very preliminary reference moon model. *J. Geophys. Res. Planets*, *188*(1-2), 96–113. doi: 10.1016/j.pepi.2011.06.015
- Garcia, R. F., Gagnepain-Beyneix, J., Chevrot, S., & Lognonné, P. (2012). Erratum to “very preliminary reference moon model”. *Phys. Earth Planet. Inter.*, *202-203*, 89–91. doi: 10.1016/j.pepi.2012.03.009
- Giguere, T. A., Boyce, J. M., Gillis-Davis, J. J., Trang, D., & Stopar, J. D. (2022). Lava flow ages in northeastern oceanus procellarum: The need for calibrating crater counting procedures. *Icarus*, *375*, 114838. doi: 10.1016/j.icarus.2021.114838
- Guerrero, J. M., Lowman, J. P., Deschamps, F., & Tackley, P. J. (2018). The influence of curvature on convection in a temperature-dependent viscosity fluid: Implications for the 2-d and 3-d modeling of moons. *J. Geophys. Res. Planets*, *123*, 1863–1880. doi: 10.1029/2017JE005497
- Hamid, S. S., O’rourke, J. G., & Soderlund, K. M. (2023). A long-lived lunar magnetic field powered by convection in the core and a basal magma ocean. *Planet. Sci. J.*, *4*(5), 88. doi: 10.3847/PSJ/acb99
- Head, J. W., & Wilson, L. (2017). Generation, ascent and eruption of magma on the moon: new insights into source depths, magma supply, intrusions and effusive/explosive eruptions (part 2: predicted emplacement processes and observations). *Icarus*, *283*, 176–223. doi: 10.1016/j.icarus.2016.05.031
- Head, J. W., & Wilson, L. (2020). Magmatic intrusion-related processes in the upper lunar crust: The role of country rock porosity/permeability in magmatic percolation and thermal annealing, and implications for gravity signatures. *Planetary and Space Science*, *180*(104765). doi: 10.1016/j.pss.2019.104765
- Head, J. W., Wilson, L., Hiesinger, H., van der Bogert, C., Chen, Y., Dickson, J. L., ... others (2023). Lunar mare basaltic volcanism: Volcanic features and emplacement processes. *Rev. Mineral. Geochem.*, *89*(1), 453–507. doi: 10.2138/rmg.2023.89.11
- Hess, P. C., & Parmentier, E. M. (1995). A model for the thermal and chemical evolution of the moon’s interior: implications for the onset of mare volcanism. *Earth Planet. Sci. Lett.*, *134*(3–4), 501–514. doi: 10.1016/0012-821X(95)00138-3
- Hiesinger, H., Head III, J. W., Wolf, U., Jaumann, R., & Neukum, G. (2003). Ages and stratigraphy of mare basalts in oceanus procellarum, mare nubium, mare cognitum, and mare insularum. *J. Geophys. Res. Planets*, *108*(E7), 5065. doi: 10.1029/2002JE001985
- Hiesinger, H., Jaumann, R., Neukum, G., & Head, J. W. (2000). Ages and stratigraphy of mare basalts in oceanus procellarum, mare nubium, mare cognitum, and mare insularum. *J. Geophys. Res. Planets*, *105*(E12), 29239–29275. doi: 10.1029/2000JE001244
- Hirth, G., & Kohlstedt, D. L. (2003). Rheology of the upper mantle and the mantle wedge: A view from the experimentalists. *In Geophys. Monogr. Ser.*, *138*, 83–105. doi: 10.1029/138GM06
- Hurwitz, D. M., Head, J. W., & Hiesinger, H. (2013). Lunar sinuous rilles: Distribution, characteristics, and implications for their origin. *Planet. Space Sci.*, *79*, 1–38. doi: 10.1016/j.pss.2012.10.019
- Jolliff, B. L., Gillis, J. J., Haskin L., R. L., Korotev, & Wieczorek, M. A. (2000). Major lunar crustal terranes: Surface expressions and crustal- mantle origins. *J. Geophys. Res.*, *105*(E2), 4197–4216. doi: 10.1029/1999JE001103

- Jones, M. J., Evans, A. J., Johnson, B. C., Weller, M. B., Andrews-Hanna, J. C., Tikoo, S. M., & T., K. J. (2022). A south pole–aitken impact origin of the lunar compositional asymmetry. *Sci. Adv.*, *8*(14). doi: 10.1126/sciadv.abm8475
- Jung, J.-I., Tikoo, S. M., Burns, D., Váci, Z., & Krawczynski, M. J. (2024). Assessing lunar paleointensity variability during the 3.9–3.5 ga high field epoch. *Earth Planet. Sci. Lett.*, *638*, 118757. doi: 10.1016/j.epsl.2024.118757
- Kamata, S., Sugita, S., Abe, Y., Ishihara, Y., Harada, Y., Morota, T., . . . others (2013). Viscoelastic deformation of lunar impact basins: Implications for heterogeneity in the deep crustal paleo-thermal state and radioactive element concentration. *J. Geophys. Res. Planets*, *118*(3), 398–415. doi: 10.1002/jgre.20056
- Kameyama, M., Fujimoto, H., & Ogawa, M. (1996). A thermo-chemical regime in the upper mantle in the early earth inferred from a numerical model of magma-migration in a convecting upper mantle. *Phys. Earth Planet. Inter.*, *94*(3–4), 187–215. doi: 10.1016/0031-9201(95)03102-2
- Karato, S. (2013). Geophysical constraints on the water content of the lunar mantle and its implications for the origin of the moon. *Earth Planet. Sci. Lett.*, *384*, 144–153. doi: 10.1016/j.epsl.2013.10.001
- Kato, S., Morota, T., Yamaguchi, Y., Watanabe, S.-i., Otake, H., & Ohtake, M. (2017). Magma source transition of lunar mare volcanism at 2.3 Ga. *Meteorit. Planet. Sci.*, *52*(9), 1899–1915. doi: 10.1111/maps.12896
- Katz, R. F. (2008). Magma dynamics with the enthalpy method: Benchmark solutions and magmatic focusing at mid-ocean ridges. *Geochem. Geophys. Geosyst.*, *49*(12), 2099–2121. doi: 10.1093/petrology/egn058
- Khan, A., Connolly, J. A. D., Pommier, A., & Noir, J. (2014). Geophysical evidence for melt in the deep lunar interior and implications for lunar evolution. *J. Geophys. Res. Planets*, *119*(10), 2197–2221. doi: 10.1002/2014JE004661
- Khan, A., Maclennan, J., Taylor, S. R., & Connolly, J. A. D. (2006). Are the earth and the moon compositionally alike? inferences on lunar composition and implications for lunar origin and evolution from geophysical modeling. *J. Geophys. Res.*, *111*(E5). doi: 10.1029/2005JE002608
- Kirk, R. L., & Stevenson, D. J. (1989). The competition between thermal contraction and differentiation in the stress history of the moon. *J. Geophys. Res.*, *94*(B9), 12133–12144. doi: 10.1029/JB094iB09p12133
- Klimczak, C. (2015). Limits on the brittle strength of planetary lithospheres undergoing global contraction. *J. Geophys. Res. Planets*, *120*, 2135–2151. doi: 10.1002/2015JE004851
- Konrad, W., & Spohn, T. (1997). Thermal history of the moon: Implications for an early core dynamo and post-accretionary magmatism. *Adv. Space Res.*, *19*(10), 1511–1521. doi: 10.1016/S0273-1177(97)00364-5
- Laneuville, M., Taylor, J., & Wiczorek, M. A. (2018). Distribution of radioactive heat sources and thermal history of the moon. *J. Geophys. Res. Planets*, *123*(12), 3144–3166. doi: 10.1029/2018JE005742
- Laneuville, M., Wiczorek, M. A., Breuer, D., Aubert, J., & Ruckriemen, T. (2014). A long-lived lunar dynamo powered by core crystallization. *Earth Planet. Sci. Lett.*, *401*, 251–260. doi: 10.1016/j.epsl.2014.05.057
- Laneuville, M., Wiczorek, M. A., Breuer, D., & Tosi, N. (2013). Asymmetric thermal evolution of the moon. *J. Geophys. Res. Planets*, *118*(7), 1435–1452. doi: 10.1002/jgre.20103
- Lawrence, D. J., Feldman, W. C., Barraclough, B. L., Binder, A. B., Elphic, R. C., Maurice, S., . . . Prettyman, T. H. (2000). Small-area thorium features on the lunar surface. *J. Geophys. Res.*, *105*(E8), 20307–20331. doi: 10.1029/1999JE001177
- Le Bars, M., & Davaille, A. (2004). Whole layer convection in a heterogeneous planetary mantle. *J. Geophys. Res. Planets*, *109*(B03403). doi:



10.1029/2003JB002617

- Li, H., Zhang, N., Ling, Y., Wu, B., Dygert, N. K., Huang, J., & Parmentier, E. M. (2019). Lunar cumulate mantle overturn: a model constrained by ilmenite rheology. *J. Geophys. Res. Planets*, *124*(5), 1357–1378. doi: 10.1029/2018JE005905
- Li, Q.-L., Zhou, Q., Liu, Y., Xiao, Z., Lin, Y., Li, J.-H., ... Li, X.-H. (2021). Two-billion-year-old volcanism on the moon from chang'e-5 basalts. *Nature*, *600*, 54–58. doi: 10.1038/s41586-021-04100-2
- Liang, W., & Andrews-Hanna, J. C. (2022). Probing the source of ancient linear gravity anomalies on the moon. *Icarus*, *380*(114978). doi: 10.1016/j.icarus.2022.114978
- Liang, W., Broquet, A., Andrews-Hanna, J. C., Zhang, N., Ding, M., & Evans, A. J. (2024). Vestiges of a lunar ilmenite layer following mantle overturn revealed by gravity data. *Nat. Geosci.*, *17*, 361–366. doi: 10.1038/s41561-024-01408-2
- Lodders, K. (2003). Solar system abundances and condensation temperatures of the elements. *Astrophys J*, *591*, 1220–1247. doi: doi.org/10.1086/375492
- Lourenço, D. L., Rozel, A. B., Gerya, T., & Tackley, P. J. (2018). Efficient cooling of rocky planets by intrusive magmatism. *J. Geophys. Res.*, *11*, 322–327. doi: 10.1038/s41561-018-0094-8
- Luo, B., Wang, Z., Song, J., Qian, Y., He, Q., Li, Y., ... others (2023). The magmatic architecture and evolution of the chang'e-5 lunar basalts. *Nat. Geosci.*, *16*(4), 301–308. doi: 10.1038/s41561-023-01146-x
- Matsuyama, L., Keane, J. T., Trinh, A., Beuthe, M., & Watters, T. R. (2021). Global tectonic patterns of the moon. *Geophys. Res. Lett.*, *358*(114202). doi: 10.1016/j.icarus.2020.114202
- Maurice, M., Tosi, N., & Hüttig, C. (2024). Small-scale overturn of high-ti cumulates promoted by the long lifetime of the lunar magma ocean. *Journal of Geophysical Research: Planets*, *129*(2), e2023JE008060. doi: 10.1029/2023JE008060
- McDonough, W. F., & Sun, S.-s. (1995). The composition of the earth. *J Geophys Res Planets*, *120*, 223–253. doi: 10.1016/0009-2541(94)00140-4
- McKenzie, D. (1984). The generation and compaction of partially molten rock. *J. Petrol.*, *25*(3), 713–765. doi: 10.1093/petrology/25.3.713
- Mei, S., Bai, W., Hiraga, T., & Kohlstedt, D. L. (2002). Influence of melt on the creep behavior of olivine–basalt aggregates under hydrous conditions. *Earth Planet. Sci. Lett.*, *201*(3-4), 491–507. doi: 10.1016/S0012-821X(02)00745-8
- Miller, K. J., Zhu, W.-l., Montési, L. G. J., & Gaetani, G. A. (2014). Experimental quantification of permeability of partially molten mantle rock. *Earth Planet. Sci. Lett.*, *388*(15), 273–282. doi: 10.1016/j.epsl.2013.12.003
- Morota, T., Haruyama, J., Honda, C., Ohtake, M., Yokota, Y., Kimura, J., ... Sasaki, S. (2009). Mare volcanism in the lunar farside moscoviense region: Implication for lateral variation in magma production of the moon. *Geophys. Res. Lett.*, *36*(L21202). doi: 10.1029/2009GL040472
- Morota, T., Haruyama, J., Ohtake, M., Matsunaga, T., Honda, C., Yokota, Y., ... Hiesinger, H. (2011). Timing and characteristics of the latest mare eruption on the moon. *Earth Planet. Sci. Lett.*, *302*(3-4), 255–266. doi: 10.1016/j.epsl.2010.12.028
- Nagaoka, H., Fagan, T. J., Kayama, M., Karouji, Y., Hasebe, N., & Ebihara, M. (2020). Formation of ferroan dacite by lunar silicic volcanism recorded in a meteorite from the moon. *Prog. Earth Planet. Sci.*, *7*, 1–18. doi: 10.1186/s40645-020-0324-8
- Ogawa, M. (2018a). The effects of magmatic redistribution of heat producing elements on the lunar mantle evolution inferred from numerical models that start from various initial states. *Planet. Space Sci.*, *151*, 43–55. doi: 10.1016/j.pss.2017.10.015
- Ogawa, M. (2018b). Magmatic differentiation and convective stirring of the mantle



- in early planets: the effects of the magmatism-mantle upwelling feedback. *Geophys. J. Int.*, 215(3), 2144–2155. doi: 10.1093/gji/ggy413
- Ogawa, M. (2020). Magmatic differentiation and convective stirring of the mantle in early planets – 2: effects of the properties of mantle materials. *Geophys. J. Int.*, 220(2), 1409–1420. doi: 10.1093/gji/ggz499
- Parmentier, E. M., Zhong, S., & Zuber, M. T. (2002). Gravitational differentiation due to initial chemical stratification: origin of lunar asymmetry by the creep of dense creep? *Earth Planet. Sci. Lett.*, 201, 473–480. doi: 10.1016/S0012-821X(02)00726-4
- Ringwood, A. E., & Kesson, S. E. (1976). A dynamic model for mare basalt petrogenesis. *Proc. Lunar Sci. Conf.*, 7, 1697–1722.
- Sakamaki, T., Ohtani, E., Urakawa, S., Suzuki, S., Katayama, Y., & Zhao, D. (2010). Density of high-ti basalt magma at high pressure and origin of heterogeneities in the lunar mantle. *Earth Planet. Sci. Lett.*, 299(3-4), 285–289. doi: 10.1016/j.epsl.2010.09.007
- Sato, H., Robinson, M. S., Lawrence, S. J., Denevi, B. W., Hapke, B., Jolliff, B. L., & Hiesinger, H. (2017). Lunar mare tio2 abundances estimated from uv/vis reflectance. *Icarus*, 296, 216–238. doi: 10.1016/j.icarus.2017.06.013
- Sawada, N., Morota, T., Kato, S., Ishihara, Y., & Hiramatsu, Y. (2016). Constraints on timing and magnitude of early global expansion of the moon from topographic features in linear gravity anomaly areas. *Geophys. Res. Lett.*, 43(10), 4865–4870. doi: 10.1002/2016GL068966
- Scheinberg, A. L., Soderlund, K. M., & Elkins-Tanton, L. T. (2018). A basal magma ocean dynamo to explain the early lunar magnetic field. *Earth and Planetary Science Letters*, 492, 144–151. doi: 10.1016/j.epsl.2018.04.015
- Schwinger, S., & Breuer, D. (2022). Employing magma ocean crystallization models to constrain structure and composition of the lunar interior. *Phys. Earth Planet. Inter.*, 322. doi: 10.1016/j.pepi.2021.106831
- Scott, T., & Kohlstedt, D. L. (2006). The effect of large melt fraction on the deformation behavior of peridotite. *In Geophys. Monogr. Ser.*, 246, 177–187. doi: 10.1016/j.epsl.2006.04.027
- Shearer, C. K., Hess, P. C., Wieczorek, M. A., Pritchard, M. E., Parmentier, E. M., Borg, L. E., . . . Wiechert, U. (2006). Thermal and magmatic evolution of the moon. *Rev Mineral Geochem*, 60(1), 365–518. doi: doi.org/10.2138/rmg.2006.60.4
- Siegler, M. A., & Smrekar, S. E. (2014). Lunar heat flow: Regional perspective of the apollo landing sites. *J. Geophys. Res. Planets*, 119(1), 47–63. doi: 10.1002/2013JE004453
- Siegler, M. A., Warren, P., Franco, K. L., Paige, D., Feng, J., & White, M. (2022). Lunar heat flow: Global predictions and reduced heat flux. *J. Geophys. Res. Planets*, 127(e2022JE007182). doi: 10.1029/2022JE007182
- Snyder, G. A., Taylor, L. A., & Neal, C. R. (1992). A chemical model for generating the sources of mare basalts: Combined equilibrium and fractional crystallization of the lunar magmasphere. *Geochim. Cosmochim. Acta*, 56(10), 3809–3823. doi: 10.1016/0016-7037(92)90172-F
- Solomon, S. C., & Chaiken, J. (1976). Thermal expansion and thermal stress in the moon and terrestrial planets: clues to early thermal history. *Proc. Lunar Sci. Conf.*, 7, 3229–3243.
- Solomon, S. C., & Head, J. W. (1979). Vertical movement in mare basins: Relation to mare emplacement, basin tectonics, and lunar thermal history. *J. Geophys. Res.*, 84(B4), 1667–1682. doi: 10.1029/JB084iB04p01667
- Solomon, S. C., & Toksöz, M. N. (1973). Internal constitution and evolution of the moon. *Phys. Earth Planet. Inter.*, 7(1), 15–38. doi: 10.1016/0031-9201(73)90037-X
- Spohn, T., Konrad, W., Breuer, D., & Ziethe, R. (2001). The longevity of lunar vol-

- canism: implications of thermal evolution calculations with 2d and 3d mantle convection models. *Icarus*, *149*(1), 54–65. doi: 10.1006/icar.2000.6514
- Stegman, D. R., Jellinek, A. M., Zatman, S. A., Baumgardner, J. R., & Richards, M. A. (2003). An early lunar core dynamo driven by thermochemical mantle convection. *Nature*, *421*, 143–146.
- Stys, C., & Dumberry, M. (2020). A past lunar dynamo thermally driven by the precession of its inner core. *J. Geophys. Res. Planets*, *125*(7), e2020JE006396. doi: 10.1029/2020JE006396
- Su, B., Y. J., Chen, Y., Yang, W., Mitchell, R. N., Hui, H., Wang, H., ... Wu, F.-Y. (2022). Fusible mantle cumulates trigger young mare volcanism on the cooling moon. *Sci. Adv.*, *8*(42). doi: 10.1126/sciadv.abn2103
- Taguchi, M., Morota, T., & Kato, S. (2017). Lateral heterogeneity of lunar volcanic activity according to volumes of mare basalts in the farside basins. *J. Geophys. Res. Planets*, *122*(7), 1505–1521. doi: 10.1002/2016JE005246
- Tarduno, J. A., Cottrell, R. D., Lawrence, K., Bono, R. K., Huang, W., Johnson, C. L., ... others (2021). Absence of a long-lived lunar paleomagnetosphere. *Sci. Adv.*, *7*(32), eabi7647. doi: 10.1126/sciadv.abi7647
- Taylor, G. J., & Wieczorek, M. A. (2014). Lunar bulk chemical composition: a post-gravity recovery and interior laboratory reassessment. *Philos Trans Royal Soc A*, *372*. doi: 10.1098/rsta.2013.0242
- Tian, H.-C., Zhang, C., Yang, W., Du, J., Chen, Y., Xiao, Z., ... others (2023). Surges in volcanic activity on the moon about two billion years ago. *Nat. Commun.*, *14*(1), 3734. doi: 10.1038/s41467-023-39418-0
- Tikoo, S. M., Weiss, B. P., Shuster, D. L., Suavet, C., Wang, H., & Grove, T. L. (2017). A two-billion-year history for the lunar dynamo. *Sci. Adv.*, *3*(8), e1700207. doi: 10.1126/sciadv.1700207
- Turcotte, D. L., & Schubert, G. (2014). Geodynamics. *Cambridge University Press*. doi: 10.1017/CBO9780511843877
- U, K., Hasumi, H., & Ogawa, M. (2022). Effects of magma-generation and migration on the expansion and contraction history of the moon. *Earth Planets Space*, *74*(78). doi: 10.1186/s40623-022-01631-4
- U, K., Kameyama, M., & Ogawa, M. (2023). The volcanic and radial expansion/contraction history of the moon simulated by numerical models of magmatism in the convective mantle. *J. Geophys. Res. Planets*, *128*(e2023JE007845). doi: 10.1029/2023JE007845
- van der Bogert, C. H., Clark, J. D., Hiesinger, H., Banks, M. E., Watters, T. R., & Robinson, M. S. (2018). How old are lunar lobate scarps? 1. seismic resetting of crater size-frequency distributions. *Icarus*, *306*, 225–242. doi: 10.1016/j.icarus.2018.01.019
- van Kan Parker, M., Sanloup, C., Sator, N., Guillot, B., Tronche, E. J., Perrillat, P., ... van Westrenen, W. (2012). Neutral buoyancy of titanium-rich melts in the deep lunar interior. *Nat. Geosci.*, *5*, 186–189. doi: 10.1038/ngeo1402
- Watters, T. R., Robinson, M. S., Beyer, R. A., Banks, M. E., Bell, J. F., Pritchard, M. E., ... Williams, N. R. (2010). Evidence of recent thrust faulting on the moon revealed by the lunar reconnaissance orbiter camera. *Science*, *329*(5994), 936–940. doi: 10.1126/science.1189590
- Watters, T. R., Robinson, M. S., Collins, G. C., Banks, M. E., Daud, K., Williams, N. R., & Selvens, M. M. (2015). Global thrust faulting on the moon and the influence of tidal stresses. *Geology*, *43*(10), 851–854. doi: 10.1130/G37120.1
- Weiss, B. P., & Tikoo, S. M. (2014). The lunar dynamo. *Science*, *346*(6214), 1246753. doi: 10.1126/science.1246753
- Whitten, J. L., & Head, J. W. (2015). Lunar cryptomaria: Physical characteristics, distribution, and implications for ancient volcanism. *Icarus*, *247*, 150–171. doi: 10.1016/j.icarus.2014.09.031
- Wieczorek, M. A., Neumann, G. A., Nimmo, F., Kiefer, W. S., Taylor, G. J.,

- Melosh, R. J., H. J. abd Phillips, . . . Zuber, M. T. (2013). The crust of the moon as seen by grail. *Science*, *339*(6029), 671–675. doi: 10.1126/science.1199375
- Wieczorek, M. A., & Phillips, R. J. (2000). The “procellarum creep terrane”: Implications for mare volcanism and lunar evolution. *J. Geophys. Res. Planets*, *105*(E8), 20417–20430. doi: 10.1029/1999JE001092
- Wilson, L., & Head, J. W. (2003). Deep generation of magmatic gas on the moon and implications for pyroclastic eruptions. *Icarus*, *30*(12). doi: 10.1029/2002GL016082
- Wilson, L., & Head, J. W. (2017). Generation, ascent and eruption of magma on the moon: new insights into source depths, magma supply, intrusions and effusive/explosive eruptions (part 1: theory). *Icarus*, *283*, 146–175. doi: 10.1016/j.icarus.2015.12.039
- Wood, J. A. (1972). Thermal history and early magmatism in the moon. *Icarus*, *16*(2), 229–240. doi: 10.1016/0019-1035(72)90070-X
- Xu, M., Jing, Z., Van Orman, J. A., Yu, T., & Wang, Y. (2022). Experimental evidence supporting an overturned iron-titanium-rich melt layer in the deep lunar interior. *Geophys. Res. Lett.*, *49*(13). doi: 10.1029/2022GL099066
- Yu, S., Tosi, N., Schwinger, S., Maurice, M., Breuer, D., & Xiao, L. (2019). Overturn of ilmenite-bearing cumulates in a rheologically weak lunar mantle. *J. Geophys. Res. Planets*, *124*(2), 418–436.
- Yue, Z., Michael, G. G., Di, K., & Liu, J. (2017). Global survey of lunar wrinkle ridge formation times. *Earth Planet. Sci. Lett.*, *477*, 14–20. doi: 10.1016/j.epsl.2017.07.048
- Zhang, D., Su, B., Chen, Y., Yang, W., Mao, Q., & Jia, L.-H. (2022). Titanium in olivine reveals low-ti origin of the chang’e-5 lunar basalts. *Lithos*, *414*, 106639. doi: 10.1016/j.lithos.2022.106639
- Zhang, N., Ding, M., Zhu, M.-H., Li, H., Li, H., & Yue, Z. (2022). Lunar compositional asymmetry explained by mantle overturn following the south pole–aitken impact. *Nat. Geosci.*, *15*, 37–41. doi: 10.1038/s41561-021-00872-4
- Zhang, N., Dygert, N., Liang, Y., & Parmentier, E. (2017). The effect of ilmenite viscosity on the dynamics and evolution of an overturned lunar cumulate mantle. *Geophys. Res. Lett.*, *44*, 6543–6552. doi: 10.1002/2017GL073702
- Zhang, N., Parmentier, E., & Liang, Y. (2013a). A 3-d numerical study of the thermal evolution of the moon after cumulate mantle overturn: the importance of rheology and core solidification. *J. Geophys. Res. Planets*, *118*(9), 1789–1804. doi: 10.1002/jgre.20121
- Zhang, N., Parmentier, E., & Liang, Y. (2013b). Effects of lunar cumulate mantle overturn and megaregolith on the expansion and contraction history of the moon. *Geophys. Res. Lett.*, *40*(19), 5019–5023. doi: 10.1002/grl.50988
- Zhang, W., Zhang, N., & Li, H. Y. (2022). Abundances of lunar heat-producing elements constrained by a 3-d numerical model of titanium-rich basaltic eruption. *Chinese J. Geophys.*, *65*(1), 119–136. doi: 10.6038/cjg2022P0753
- Zhang, W., Zhang, N., Liang, Y., & Togle, L. (2023). The effect of pressure-dependent viscosity on the dynamics of the post-overturn lunar mantle. *J. Geophys. Res. Planets*, *128*(10), e2023JE007933. doi: 10.1029/2023JE007933
- Zhao, Y., de Vries, J., van den Berg, A. P., Jacobs, M. H. G., & van Westrenen, W. (2019). The participation of ilmenite-bearing cumulates in lunar mantle overturn. *Earth Planet. Sci. Lett.*, *511*(1), 1–11. doi: 10.1016/j.epsl.2019.01.022
- Zhong, S., Parmentier, E. M., & Zuber, M. T. (2000). A dynamic origin for the global asymmetry of lunar mare basalts. *Earth Planet. Sci. Lett.*, *177*(3–4), 131–140. doi: 10.1016/S0012-821X(00)00041-8
- Ziethe, R., Seiferlin, K., & Hiesinger, H. (2009). Duration and extent of lunar volcanism: Comparison of 3d convection models to mare basalt ages. *Planet. Space Sci.*, *57*(7), 784–796. doi: 10.1016/j.pss.2009.02.002

### **Acknowledgments**

The authors would like to extend their sincere appreciation to M. Kayama at the University of Tokyo and T. Yanagisawa at JAMSTEC for their constructive comments. This work was supported by JST SPRING Grant Number JP-MJSP2108 and JSPS KAKENHI Grant Number JP202412823 of Japan. This work was also supported by: the Joint Usage/Research Center PRIUS at Ehime University, the Earth Simulator of Japan Agency for Marine-Earth Science and Technology (JAMSTEC), “Exploratory Challenge on Post-K Computer” (Elucidation of the Birth of Exoplanets [Second Earth] and the Environmental Variations of Planets in the Solar System), and “Program for Promoting Research on the Supercomputer Fugaku” (Toward a unified view of the universe: from large scale structures to planets). This work used computational resources of the supercomputer Fugaku provided by the RIKEN Center for Computational Science through the HPCI System Research Project (Project ID: hp230204, hp240219). Animations and some figures were drawn with the ParaView by Sandia National Laboratory, Kitware Inc., and Los Alamos National Laboratory.